RESEARCH

Molecular and spatial heterogeneity of microglia in Rasmussen encephalitis

Jesse J. Westfall[1], Wesley N. Schwind[1], Sahibjot Sran[1], Jason B. Navarro[1], Jeffrey Leonard[2,3], Jonathan A. Pindrik[2,3], Christopher R. Pierson[4,5,6], Daniel R. Boué[4,5], Daniel C. Koboldt[1,7], Adam P. Ostendorf[3,7,8], Richard K. Wilson[1,7], Elaine R. Mardis[1,3,7], Katherine E. Miller[1,7]* and Tracy A. Bedrosian[1,7]*

Abstract

Rasmussen encephalitis (RE) is a rare childhood neurological disease characterized by progressive unilateral loss of function, hemispheric atrophy and drug-resistant epilepsy. Affected brain tissue shows signs of infiltrating cytotoxic T-cells, microglial activation, and neuronal death, implicating an inflammatory disease process. Recent studies have identified molecular correlates of inflammation in RE, but cell-type-specific mechanisms remain unclear. We used single-nucleus RNA-sequencing (snRNA-seq) to assess gene expression across multiple cell types in brain tissue resected from two children with RE. We found transcriptionally distinct microglial populations enriched in RE compared to two age-matched individuals with unaffected brain tissue and two individuals with Type I focal cortical dysplasia (FCD). Specifically, microglia in RE tissues demonstrated increased expression of genes associated with cytokine signaling, interferon-mediated pathways, and T-cell activation. We extended these findings using spatial proteomic analysis of tissue from four surgical resections to examine expression profiles of microglia within their pathological context. Microglia that were spatially aggregated into nodules had increased expression of dynamic immune regulatory markers (PD-L1, CD14, CD11c), T-cell activation markers (CD40, CD80) and were physically located near distinct CD4+ and CD8+ lymphocyte populations. These findings help elucidate the complex immune microenvironment of RE.

Keywords: Encephalitis, Microglial nodules, Epilepsy, Inflammation, Spatial proteomics, Single nucleus RNA-seq, Cytokine signaling

Introduction

Rasmussen encephalitis (RE) is a rare, progressive neurological disease characterized by intractable seizures and unilateral neurological deficits with atrophy of the contralateral cerebral hemisphere [62]. The disorder mainly affects children, with a median onset around 6 years of age, and an estimated incidence of 1.7 to 2.4 cases per 10 million children [10]. The etiology of RE is unknown,

but the evidence points to an immunopathological mechanism, particularly involving T-cell cytotoxicity and microglial activation. On histopathologic examination, brain tissue from RE patients typically shows signs of cortical inflammation, infiltrating cytotoxic T-cells, microglial nodules, neuronal loss, and gliosis in the affected hemisphere [48]. As the disease progresses, cortical cavitation and profound degeneration are observed [44].

RE remains a disease with poorly understood etiology [17, 58]. For a decade, studies have implicated microglia and their interaction with infiltrating T-cells in RE disease progression and neurodegeneration [42, 43, 62]. The quantification of these intercellular mechanisms, and their contributions to RE pathogenesis, has remained elusive. Omics analysis at tissue resolution and traditional

*Correspondence: Katherine.Miller@Nationwidechildrens.org; Tracy.
Bedrosian@Nationwidechildrens.org

[1] The Steve and Cindy Rasmussen Institute for Genomic Medicine, Abigail Wexner Research Institute at Nationwide Children's Hospital, Research Building 3, 575 Children's Crossroad, Columbus, OH 43215, USA
Full list of author information is available at the end of the article

Westfall *et al. Acta Neuropathologica Communications*   (2022) 10:168

Page 2 of 16

low-plex immunohistochemistry have made incremental advances to elucidate the complex network of cytokine-mediated signaling driving the inflammatory immune response, but much remains to be determined. Diagnostic challenges further obscure the origin of RE pathogenicity, particularly in early-stage RE. Lacking distinct disease biomarkers, diagnosis relies on clinical, morphological and electrophysiological criteria [41]. Atypical presentation can elude clinical diagnosis and there are no specific EEG abnormalities that can distinguish RE from other focal epilepsy [41, 58]. Neuroimaging is used to identify the unilateral inflammation and atrophy that characterizes RE but is often negative in early stages [62]. These shortcomings highlight the need for high-resolution, multiomic analyses.

Several studies have characterized aspects of innate and adaptive immune activity in RE. At early disease stages, there is an upregulation of innate immune response including MHC-class-1 antigen presentation and interferon signaling [60]. The formation of small microglial nodules expressing Toll-like receptor 7 precedes infiltration of lymphocytes to the brain. As the disease progresses, gene expression of chemokines responsible for T-cell attraction, such as *CCL5*, *CXCL9*, and *CXCL20*, are more abundantly expressed in RE patient brains, as well as inflammatory gene expression including *IL-1β* and *IFNγ* [43, 60]. Infiltration and clonal T-cell expansion occurs in the brains of RE patients and CD8 + cytotoxic T-cells localize to the microglial nodules [1, 52, 53]. These T-cells can be observed closely apposed to neurons, where it is believed they may recognize a specific epitope that is yet to be identified [53].

These findings suggest that the microglial response is a key component of RE pathogenesis, but studies so far have relied on bulk tissue gene expression assays that do not allow for cell-type resolution. Here we applied single-nucleus RNA-sequencing (snRNA-seq) to identify cell-type-specific gene expression changes in RE, with a particular focus on microglia. We extended these findings by applying spatial proteomic assays to study expression of microglia within their pathological context. Our results help elucidate the complex immune microenvironment of RE.

Materials and methods
Patient cohort
Samples RE1, RE2, RE3, FCD1 and FCD2 were collected from patients diagnosed with either Rasmussen encephalitis (RE) or Type I focal cortical dysplasia (FCD) and enrolled in an IRB-approved research study at Nationwide Children's Hospital. Samples RE2 and RE3 originated from the same patient, but from different surgeries three years apart over the course of disease progression. Formalin-fixed, paraffin embedded (FFPE) tissue samples for RE4 were obtained from the Cooperative Human Tissue Network, a resource supported by the National Cancer Institute. Samples CTRL1 and CTRL2 were collected from unaffected donors at autopsy courtesy of the NIH Neurobiobank. See Table 1 for details.

Single-nucleus RNA-sequencing
Nuclei isolation
Nuclei were isolated from frozen brain tissue as previously described [29]. Briefly, ~ 20 mg of tissue was

Table 1 Sample information

Sample ID	Patient Age at Surgery	Sex	Diagnosis	Sample origin	Brain region studied	Frozen tissue for snRNA-seq	FFPE slides for spatial proteomics
RE1	0–5	F	RE	Left-sided functional hemispherectomy	Anterior temporal lobe	X	X
RE2	6–10	F	RE	Left anterior temporal lobectomy	Anterior temporal lobe		X
RE3	6–10	F	RE	Left peri-insular functional hemispherectomy	Posterior temporal lobe	X	X
RE4	6–10	F	RE	Right anatomic hemispherectomy	Temporal lobe		X
FCD1	11–15	F	FCD Type I	Excision of left superior parietal and occipital lobe	Superior parietal and occipital lobe	X	
FCD2	11–15	F	FCD Type I	Resection of right inferior parietal epileptic zone	Middle frontal gyrus	X	
CTRL1	0–5	F	Deceased (Lymphocytic Myocarditis)	Autopsy – temporal cortex (Brodmann area 22)	Temporal cortex	X	
CTRL2	0–5	F	Deceased (Respiratory Failure)	Autopsy – temporal cortex (Brodmann area 22)	Temporal cortex	X	

mechanically homogenized using a glass Dounce homogenizer. Nuclei were washed and stained with Hoechst 33,342 dye (Thermo Fisher Scientific #62,249), filtered through a 30 μm mesh filter, and resuspended in PBS. FACS analysis was performed using an Influx Cell Sorter (BD Biosciences). Cellular debris were excluded using forward and side scatter area parameters, nuclei were gated on Hoechst-positive signal, and then aggregates were excluded using trigger pulse width. Purified Hoechst-positive nuclei were sorted directly into 10x Genomics reaction buffer and processed according to the manufacturer protocol for Chromium Next GEM Single-Cell 3'-Reagent Kit v.3.1. Final libraries were sequenced either on an Illumina NovaSeq 6000 or HiSeq 4000 instrument to generate paired-end sequencing data.

Data pre-processing
Generation of FASTQ files, read alignment to the GRCh38 transcriptome and quantification of cell feature counts was performed using 10x Genomics Cell Ranger v.6.0 following default parameters, except for inclusion of intronic transcripts, which are present in nucleic pre-mRNAs.

$$Normalization\ \text{Factor}(NF) = \frac{(nuclei\ in\ sample)}{(nuclei\ in\ sample\ with\ largest\ number\ of\ nuclei)}$$

$$normalized\ cell\ number = \frac{(number\ of\ nuclei\ in\ cell\ type\ cluster\ in\ a\ sample)}{NF}$$

Quality filtering, normalization, and integration
Downstream analysis was performed using Seurat v4.0 for R [23]. Briefly, cell-barcode gene expression matrices were filtered to contain genes that were expressed in at least three nuclei and to contain nuclei that express at least 1000 transcripts of 500 unique genes. Nuclei with greater than 5% mitochondrial transcripts were filtered out. Normalization and variance-stabilization of feature-barcode matrices were performed using the sctransform package for R [22]. Nuclear doublets were detected and eliminated from the data via DoubletFinder v2.0 [36]. Feature-barcode matrices were integrated using the IntegrateData function in Seurat.

Dimensionality reduction, clustering and visualization
Principal component analysis (PCA) was performed using Seurat v.4.0. The first 30 PCs were used to generate a shared nearest neighbor (SSN) graph by calculating the Jaccard Index between every nucleus and its 20 nearest neighbors. The resulting SSN graph was used to perform

Louvain clustering [59]. Gene expression profiles were visualized in two-dimensional space using t-distributed stochastic neighbor embedding (tSNE) [61].

Cell type annotation
Cell types were annotated using the reference-query label transfer method in Seurat v.4.0 using human cortical single-nuclei gene expression data from the Allen Brain Map M1 10x dataset [7]. Briefly, a set of transfer anchors is calculated from the PCA reduction of each dataset. Then, each nucleus in the query dataset is scored on a reference vector of cell type labels, generating a matrix of prediction scores and predicted IDs to be added to the query's metadata. To confirm predicted cell types and find nuclei from non-resident nuclei, canonical cell type markers were visualized with the Nebulosa v3.14 R package [2].

Normalized cell type quantification
To correct for sample size when reporting cell type proportions, the number of nuclei in each cell type cluster was normalized to total nuclei in each sample using the following formulas, as previously published [51].

Subclustering and differential gene expression
Microglia were subset from the integrated Seurat object and reprocessed using normalization, integration, dimensional reduction, and clustering steps as described above. To discover differentially expressed genes (DEGs) between disease conditions, we used the pseudobulk method of aggregating gene expression across cells of biological replicates, then employed DESeq2 to test for differential expression [33]. Dimensionality reduction, Louvain clustering and visualization were performed using Seurat v.4.0 as described above. Highly expressed genes were discovered on a per-cluster basis using the FindAllMarkers function in Seurat v.4.0 with test.use set to Model-based Analysis of Single-cell Transcriptomics (MAST) [18].

GO Enrichment and KEGG Pathway analysis
Gene Ontology enRIchment anaLysis and visuaLizAtion tool (GOrilla) was used to analyze DEGs in microglia across disease conditions and across microglia

clusters [15]. All genes with transcripts sequenced across the RE, FCD1 and CTRL samples were used as a background list. DEGs were queried for enriched Gene Ontology (GO) biological process annotations (FDR adjusted *p*-value < 0.05). Additionally, microglial DEGs across disease conditions were input into the Kyoto Encyclopedia of Genes and Genomes (KEGG) Pathway Database Mapper Search Tool [25] for pathway analysis and visualization.

Cell typing statistics

To test significance of microglial cluster association to disease condition, an entropy based metric, the cell type diversity statistic (CTDS) was employed [26]. CTDSs were normally distributed and maintained homogeneity of variance, confirmed by Shapiro–Wilk test and Bartlett's test respectively, and tested via one-way ANOVA.

Trajectory analysis

Trajectory analysis was performed via Monocle3 [46]. Microglia were dimensionally reduced via Uniform Manifold Approximation and Projection (UMAP) with Seurat v.4.0. Using UMAP loading scores and Louvain clusters, cells were ordered along computationally generated pseudotime trajectories using the 'learn_graph' and 'order_cells' functions. Differentially expressed genes across pseudotime were found by spatial autocorrelation (Moran's I test) using the 'graph_test' function.

Digital spatial proteomics

Slide preparation

FFPE tissue sections (5 µm thick) were processed according to the GeoMx® Digital Spatial Profiler (DSP) protocol (NanoString Technologies, Inc.). Briefly, tissue was deparaffinized and rehydrated with CitriSolv (Decon Labs), ethanol and ddH_2O washes at room temperature. Antigen retrieval was performed in citrate buffer pH 6.0

and CD45-AF594 (NanoString Technologies, Inc. #121,300,301) and the following oligo-tagged NanoString GeoMx human detection antibody mixtures: Immune Core Profiling, Immune Cell Typing, Immune Activation, and Cell Death (see Supplemental Material for list of detection targets). Slides were washed with TBS-T, fixed with 4% formaldehyde (Invitrogen) for 1 h at room temperature, then re-washed with TBS-T. Nuclei were stained with SYTO 13 (NanoString).

GeoMx instrument use and analysis

Slides were scanned in a GeoMx DSP instrument. Geometric regions of interest (ROIs) were selected and segmented for each tissue section, focusing on areas containing microglial nodules and aggregated immune cells. For each ROI, CD45+ segment borders were generated by manually selecting a CD45 fluorescence threshold that visually maximized, based on intensity and cell morphology, inclusion of invading immune cells while excluding microglia. Subsequently, IBA1+ segment borders were generated by manually selecting an IBA1 fluorescence threshold that visually maximized inclusion of microglia while excluding non-cellular area. Oligos from selected ROI segments were cleaved, collected and dried in a 96-well plate. Oligos were hybridized to unique reporter tags and counted with the Nanostring nCounter platform following the manufacturer protocol. The number of selected ROI segments per sample is detailed in Table 2.

Data quality control, normalization and differential expression analysis were performed on NanoString GeoMx Software v2.4 following manufacturer recommendations. Differentially expressed proteins were determined by Mann Whitney U Test with *p*-values corrected by Benjamini–Hochberg procedure (*p* < 0.05). Relative expression of cell type markers and cell activation markers was calculated as follows:

$$\text{Cell marker \% Counts} = \frac{\text{\# of oligos from specific cell type marker}}{\text{total \#of oligos from all cell type markers}} \times 100$$

$$\text{Cell activation \% Counts} = \frac{\text{\# of oligos from specific cell activation marker}}{\text{total \#of oligos from all cell activation markers}} \times 100$$

(Millipore) at ~115 °C under high pressure and washed in tris-buffered saline with Tween 20 (TBS-T) (Cell signaling Technology). Tissue was blocked with Buffer W (Nanostring) for 1 h at room temperature. Slides were incubated at 4 °C overnight with antibody mixture including fluorescently tagged antibodies for IBA1-AF532 (Nanostring Technologies, Inc. #121,300,306)

Immunohistochemistry

Formalin-fixed paraffin-embedded tissue sections (5 µm thick) were processed according to the GeoMx Digital Spatial Proteomics protocol (NanoString Technologies, Inc.), as above, with the addition of CD8-AF647 (Novus #NBP2-54595AF647)

Westfall *et al. Acta Neuropathologica Communications*   (2022) 10:168

Page 5 of 16

Table 2 GeoMx sample ROI information

Sample Name	Slide #	# IBA1+ROI segments	# CD45+ROI segments
RE1	1	13	10
RE1	2	21	15
RE2	1	14	10
RE2	2	11	7
RE3	1	15	9
RE3	2	11	7
RE4	1	14	10
RE4	2	13	9

and the exclusion of GeoMx human detection antibodies. High-resolution full-slide images at 20 × were obtained via the GeoMx DSP.

Microglial expansion and infiltrating lymphocytes in RE

To determine the cell type composition of RE-affected cortical tissue, we performed snRNA-sequencing of frozen brain tissue from RE patients ($N=2$) compared to Type I FCD patients ($N=2$) and unaffected donors ($N=2$). FCD samples were used as an epilepsy control without any known immunological pathology, and unaffected donors had neither history of epilepsy nor immune disease. We performed unbiased nuclei isolation using mechanical dissociation and fluorescence-activated sorting for Hoechst-positive nuclei. Individual nuclei were barcoded (10xGenomics, Inc.) and cDNA libraries were sequenced (Fig. 1a). After quality control, snRNA-seq yielded 20,182 single-nuclei profiles (nuclei counts: RE=8,779; FCD=5,353; CTRL=6,050) (Additional file 1: Fig. 1a–e). An average of 2,526 genes and 6,127 transcripts per nucleus were detected. We normalized the data, applied dimensional reduction analysis and performed unbiased clustering to identify cell types (Fig. 1b–c; Aditional file 1: Fig. 1f). Nine major cell types were identified and confirmed by expression of canonical cell-type markers (Fig. 1d). Expected brain resident cell types were identified, including neurons, oligodendrocytes, astrocytes, and microglia. Microglia were highly represented in the RE patient samples, with more than twice as many identified after normalizing for sample size compared to FCD or CTRL samples. A population of non-resident, infiltrating immune cells identified with the markers CD3, SKAP1 and

CD94 originated mainly from the RE patient samples and was absent from unaffected tissue. (Fig. 1e–f; Additional file 1: Fig. 1 g-h).

Microglial gene expression in RE

We next investigated disease-specific changes in microglial gene expression using a pseudobulk comparison of RE versus both CTRL and FCD tissues in DESeq2. Pseudobulk analysis has been recently identified as a robust approach to avoid pseudo-replication bias inherent in single-cell gene expression studies [55]. Compared to CTRL tissue, our analysis revealed a total of 288 DEGs (237 with higher expression in RE samples, 51 with lower expression in RE, with at least a±1.5-fold change and an FDR-adjusted p value ≤ 0.05) (Fig. 2a, Additional file 2: Table 1). Compared to FCD tissue, our analysis revealed a total of 174 DEGs (134 with higher expression in RE samples, 40 with lower expression in RE, with at least a±1.5-fold change and an FDR-adjusted p value ≤ 0.05) (Fig. 2b, Additional file 13: Table 2). There was an overlap of 52 DEGs (39 with higher expression in RE samples, 13 with lower expression in RE) (Additional file 2: Fig. 2a-b) between the two disease-specific comparisons. Genes more abundantly expressed in RE were queried for biological process Gene Ontology (GO) annotation enrichment. Both sets of DEGs showed enrichment for immune mediation, including pathways for T-cell activation and cytokine signaling. In particular, DEGs highly expressed in RE vs. FCD were enriched for multiple interferon-mediated pathways, MHCI/II antigen presentation, CD8+/CD4+T-cell activation and Toll-like receptor pathways (Fig. 2c, d).

Next, we investigated the role of DEGs in well-studied biological pathways. Using the Kyoto Encyclopedia of Genes and Genomes (KEGG) Database Mapper Search Tool [25], we showed that many RE-abundant DEGs, compared to both CTRL and FCD, are in canonical immune pathways. These pathways include the TNFα pathway, known to promote inflammatory cytokine production [66] (Fig. 2e), both MHCI and MHCII components of the antigen presentation pathway (Fig. 2f) and the immune cell component of the cell adhesion pathway (Fig. 2g).

Results
Microglial heterogeneity in RE

To identify subpopulations of microglia that may be relevant to disease, we performed unbiased Louvain

(See figure on next page.)

Fig. 1 Microglial and lymphocytic cell populations are expanded in Rasmussen encephalitis. **a** Processing of cortical tissue from RE ($N=2$), FCD ($N=2$), and unaffected ($N=2$) individuals for snRNA-seq was performed using 10x Genomics 3′gene expression kit. **b** tSNE plot highlighting patient contribution to each cluster. **c** tSNE plots overlaid with feature density for canonical cell type markers (endothelial and VLMC not shown) **d** tSNE plot colored by cell type, determined using Seurat v.4.0 reference and query workflow (see methods). **e** tSNE showing contribution of diagnosis by cluster. **f** Normalized counts of nuclei per cluster by diagnosis
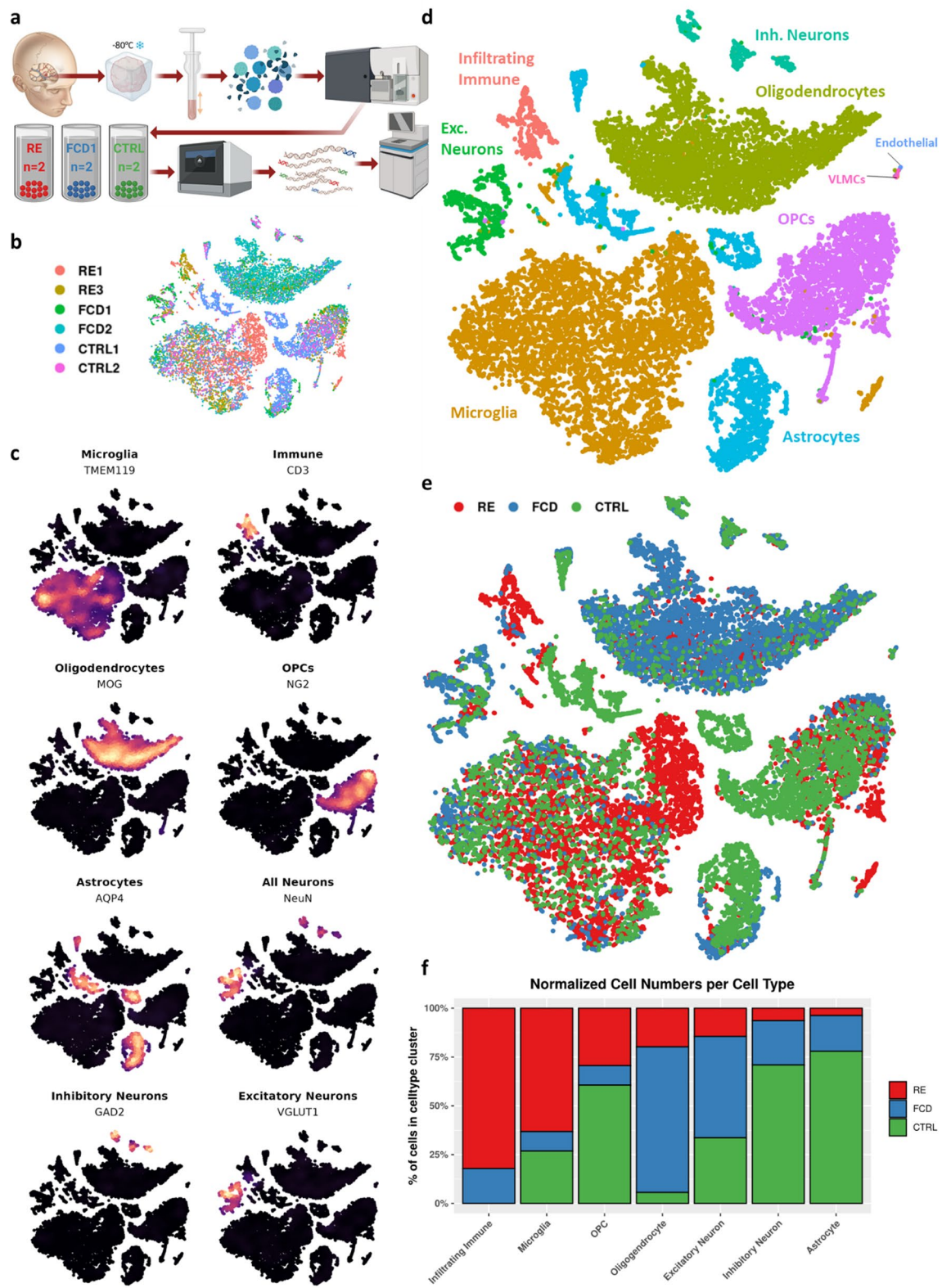
Fig. 1 (See legend on previous page.)

clustering on all microglia (Additional file 3: Fig. 3a) and determined the top differentially expressed genes for each subcluster (Additional file 3: Fig. 3b; Additional file 14: Table 3). Eleven subpopulations, or clusters, were identified. Note that each cluster, excluding cluster 7, contained cell populations from each disease condition (Additional file 4: Fig. 4a-c), though we determined that there was no statistically significant association between disease condition and microglial subpopulation (Additional file 4: Fig. 4d). Each cluster had expression of microglia-specific and homeostatic markers (Additional file 3: Fig. 3c). However, clusters 0 and 4 returned no significant DEGs and cluster 5 DEGs were nearly all ribosomal or mitochondrial genes. The remaining eight subpopulations had highly expressed gene markers involved in immune or inflammatory processes (Fig. 3ab) and were the focus of further analysis. Most of these eight clusters were defined by well-known pro-inflammatory markers. However, one population (Fig. 3b, cluster 6) was characterized by anti-inflammatory gene markers *CD163* and *MRC1*. Many of these markers, particularly in clusters 6,7,8 and 9, were more highly expressed in the RE microglia than the CTRL and FCD microglia (Additional file 5: Fig. 5).

DEGs in each cluster were queried for enriched biological process GO annotations. Six of the clusters were enriched for at least one GO term (Fig. 3c). Cluster 1 was enriched for apoptotic and cell death markers. Clusters 3 and 6 were enriched for regulation of immune processes including activation of immune cells (CD4+/CD8+ T-cells, neutrophils) and inflammatory cytokine (*IL-12*, Type I interferon) production. Cluster 2 was enriched for regulation of macrophage derived foam cell differentiation, cells which have been implicated as pro-inflammatory in multiple neuroinflammatory disorders [68]. Clusters 7 and 10 were enriched for regulation of neuronal organization and signaling, including glutamate signaling pathways and glutamatergic synaptic transmission. Disruptions in homeostatic glutamate levels and signaling have been linked to excitotoxic damage from chronic seizures across a range of pathologies [8].

To examine the relationship between homeostatic microglia and immune-regulatory subclusters, we performed trajectory analysis. Clustered microglia were dimensionally reduced using Uniform Manifold Approximation and Projection (UMAP) (Additional file 6:

Fig. 6a). A small group of cells in cluster 4, where homeostatic marker TMEM119 expression was highest, was chosen as the root node, representing pseudotime = 0 (Additional file 6: Fig. 6b). Gene expression pseudotime trajectories were calculated, and microglia were computationally ordered along the trajectories (Additional file 6: Fig. 6c). Nearly all trajectories went from cluster 4 through cluster 0 to a terminal cluster, excluding one trajectory leading directly to cluster 10. There is also a mid-to-late pseudotime trajectory leading through clusters as follows: 0,3,2,1, with cells in cluster 1 having some of the latest pseudotime scores, along with cluster 6 (Additional file 6: Fig. 6d). Spatial autocorrelation analysis revealed 4853 pseudotime differentially expressed genes (PDEGs) over the trajectories (Additional file 15: Table 4; Top 100). Visualization of the top 20 PDEGs (Moran's I score) reveals that the PDEGs are most highly expressed in clusters 2,8,6 and 10 with many having high co-expression in clusters 8 and 10 (Additional file 7: Fig. 7). Furthermore, five of the top 20 PDEG's were also regulators of immune response or inflammation highlighted in Fig. 3b.

Spatial proteomic analysis of microglial nodules

To further profile RE microglia within their pathological context, we performed digital spatial protein profiling of brain tissue from patients using the Nanostring GeoMx platform (Additional file 8: Fig. 8a). The formation of microglial nodules in patient tissue has been reported as a key precedent to cytotoxic T-cell infiltration in RE [60]. We fluorescently labeled slides with IBA1 and CD45 to identify microglia and infiltrating lymphocytes, respectively, and compared ROIs containing microglial nodules versus unaggregated microglia within the same tissue section (Fig. 4a, Additional file 8: Fig. 8b). We quantified expression of 42 protein targets from the IBA1-positive fraction of each ROI (Additional file 9: Fig. 9) and performed differential expression analysis, which identified 14 highly differentially expressed proteins (DEPs) in microglia located in the nodules. Many of these proteins are known to be implicated in microglial activation (e.g., HLA-DR, CD80, CD40) or T-cell activity (e.g., CD8, GZMA; Fig. 4b). Indeed, immunofluorescent co-labeling of IBA1, CD45, and CD8 showed colocalization of CD8 on CD45+ lymphocytes in close proximity to microglial

(See figure on next page.)

Fig. 2 Gene expression signatures of microglia in Rasmussen encephalitis. **a** Volcano plot showing differentially expressed genes in RE vs CTRL (DESeq2 adjusted *p*-value < 0.05, FC > 1.5). Labeled genes are shown on heatmap in Fig. 2c. **b** Volcano plot showing differentially expressed genes in RE vs FCD (DESeq2 adjusted *p*-value < 0.05, FC > 1.5). Labeled genes are shown on heatmap in Fig. 2d. **c** Heatmap showing individual gene contribution (via positive fold-change) to GO biological process annotation enrichment in RE vs CTRL. **d** Heatmap showing individual gene contribution (via positive fold-change) to GO biological process annotation enrichment in RE vs FCD. **e–g** Selections from KEGG Pathways: TNF signaling pathway **e**, Antigen processing and presentation **f** and Cell adhesion molecules **g** highlighting differentially high expression of genes in RE vs both CTRL and FCD controls

Westfall *et al. Acta Neuropathologica Communications*   (2022) 10:168

Page 8 of 16
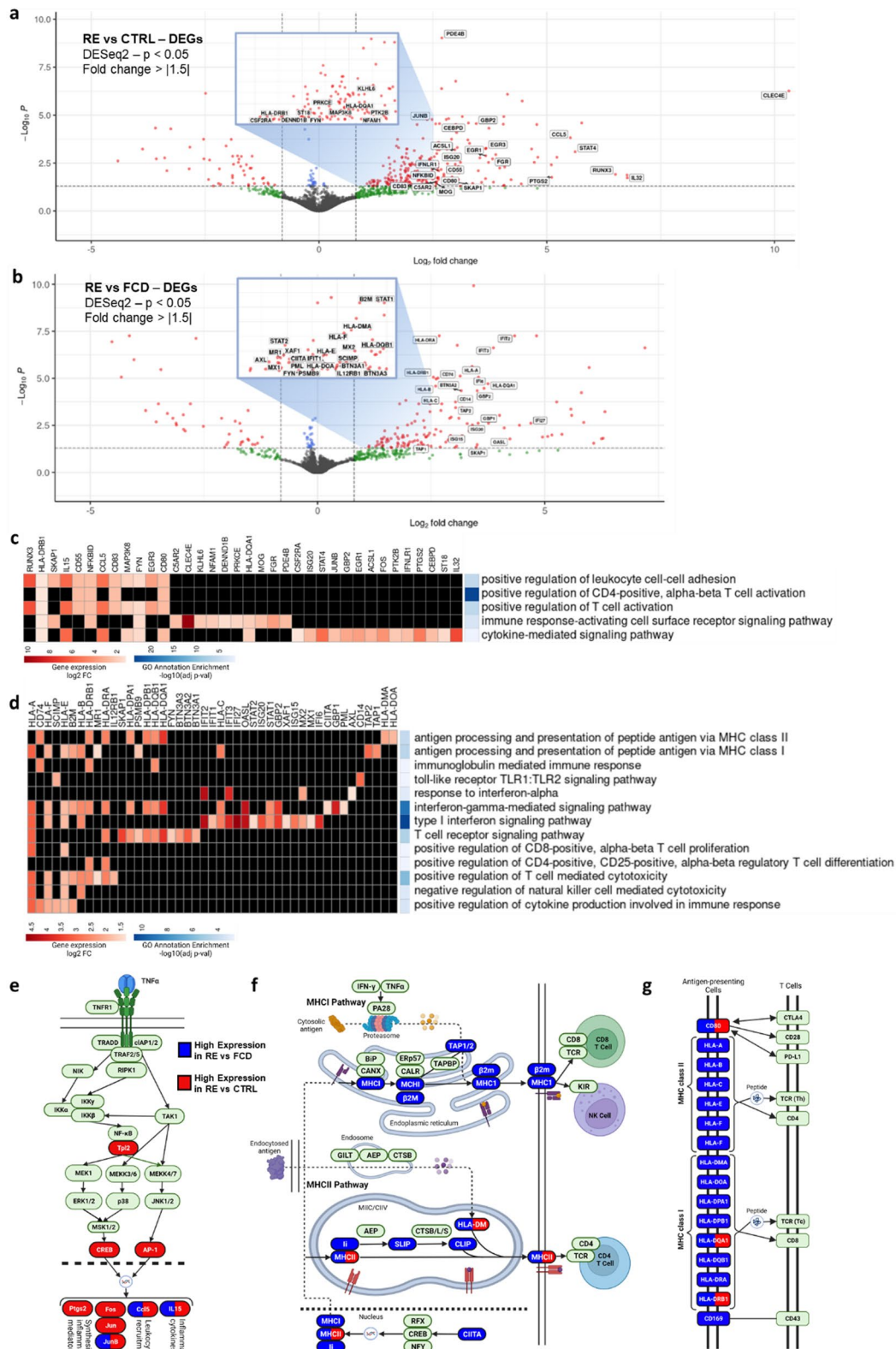
Fig. 2 (See legend on previous page.)
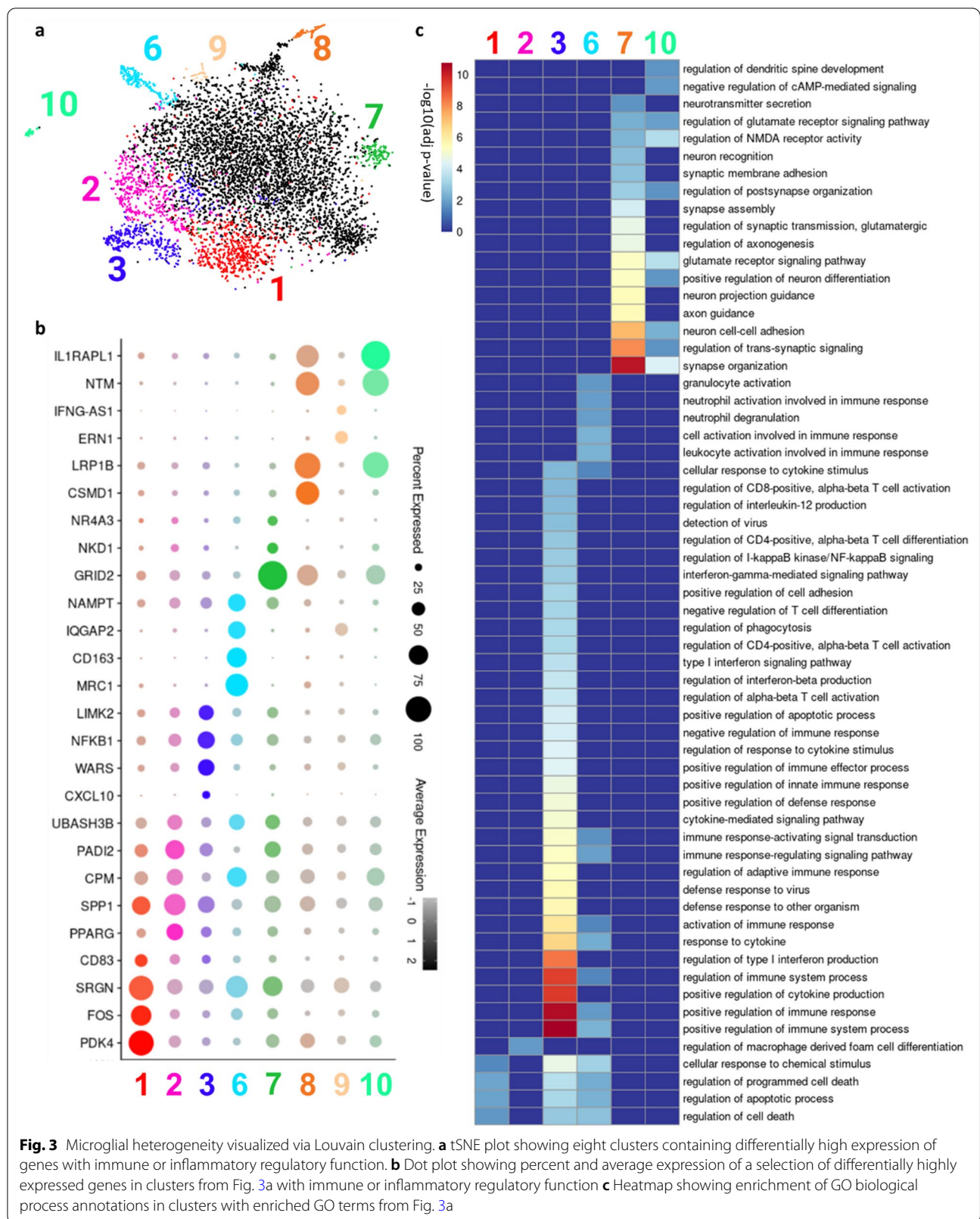
Fig. 3 Microglial heterogeneity visualized via Louvain clustering. **a** tSNE plot showing eight clusters containing differentially high expression of genes with immune or inflammatory regulatory function. **b** Dot plot showing percent and average expression of a selection of differentially highly expressed genes in clusters from Fig. 3a with immune or inflammatory regulatory function **c** Heatmap showing enrichment of GO biological process annotations in clusters with enriched GO terms from Fig. 3a

nodules (Fig. 4c). To further characterize invading immune cells localized within microglial nodules, we quantified the proportion of cell-type and cell-activation markers expressed within the CD45 + segment of the ROIs (Fig. 4d-g; Additional file 10: Fig. 10). T-cell markers dominated this signature in RE, with all four samples having evidence of CD3, CD8, CD4 expression (Fig. 4d–e). Concordantly, prominent T-cell activation markers, CD44 and HLA-DR, were highly represented in all four patients as well (Fig. 4g).

To connect spatial protein profiling to the single cell transcriptome, we analyzed a selection of six genes that encode for DEPs abundantly expressed in microglial nodules (Additional file 11: Fig. 11a). In an effort to locate microglia from a nodule in the snRNA-Seq microglia subset, the expression density of each DEP gene was plotted in the TSNE projection of the microglia (Additional file 11: Fig. 11b). A combined joint density plot revealed that some microglia in cluster 3 express all six genes that encode the microglial nodule DEPs (Additional file 11: Fig. 11c).

Discussion

In this study we applied single-nucleus transcriptomic and spatial proteomic approaches to the study of Rasmussen encephalitis resected brain tissue. Our results confirm and extend prior observations of immune-mediated pathogenesis in RE. First, we showed an expanded population of microglia and infiltrating lymphocytes in RE patients compared to brain tissue from both epilepsy-only controls and unaffected individuals. By examining the transcriptomes of microglial subclusters, we were able to identify extensive heterogeneity representing microglia in various states of activation. Finally, we were able to place that observation in pathological context by comparing expression profiles of microglia physically located within microglial nodules versus unaggregated. Microglia located in nodules expressed classic activation markers and were closely located to CD8+ T-cells.

Efforts to understand the immune-mediated pathogenicity of RE have largely focused on the study of infiltrating T-cell populations [1, 42, 52]. While microglia-associated inflammation has been studied across several different pathologies [19, 37, 54], few studies have analyzed microglial mechanisms in RE [11, 60]. Troscher et al. were the first to analyze microglial nodules in the context of RE. Our snRNA-seq differential expression analysis of RE microglia aligns with and expands on the bulk microarray gene set enrichment analysis (GSEA) of stage I and II nodules [60]. The RE microglia overexpress genes involved in MHC-I and MHC-II antigen presentation, and cytokine signaling, particularly of the interferon family. Furthermore, our data show that RE microglia have significantly higher expression of genes involved in positive regulation of specific T-cell activation, differentiation and cytotoxicity. Also, our data show support for the hypothesis that Toll-like receptors are activated upstream of immune pathways. The TLR1:TLR2 signaling pathway GO annotation is enriched in RE microglia, known to have downstream activating effects on the TNFα pathway [40]. Interestingly, in microglia, TNFα has been shown to be a potent stimulus of TLR2 expression [57], potentially creating a feedback loop for immune activation.

Performing differential expression analysis on microglial subclusters allowed us to identify and quantify the heterogeneity of microglial function in the context of RE. Looking at the most differentially expressed immune markers in each cluster revealed populations of microglia with varied inflammation profiles. Not surprisingly, there is a subset of microglia (cluster 3) with differentially high gene expression representing a pro-inflammatory Th1 immune response (*NF-κB, CXCL10*) [43, 67] and innate inflammatory responses through TLR2/4 production (*WARS1*) [38]. These cells also had high co-expression of *LIMK2*, a known biomarker for necrotic neuronal death during epileptic seizure [28]. Interestingly, a different microglial population (cluster 6) has a more ambiguous role in inflammation. Having high expression of anti-inflammatory markers *CD163* and *CD206* (*MRC1*)) [30, 50], these microglia also co-express pro-inflammatory *NAMPT* and *IQGAP2*, a ligand for, and promotor of *TLR4*, respectively [6, 20]. The dichotomy of these populations suggests a more spatially nuanced, dynamic inflammasome and implicates variation in Toll-like receptor signaling as potential mediator, reinforcing previous observations made by Luan et al. [34]. It is important to note that while microglia from all microglial subclusters were represented in each disease condition, there was an overall increased proportion of microglia in RE compared to the other conditions (Additional file 4:

(See figure on next page.)

Fig. 4 Microglia have distinct expression signatures based on spatial context in Rasmussen encephalitis. **a** Example ROIs representing a microglial nodule (left, yellow) versus unaggregated microglia (right, light blue) with immunofluorescent staining of microglia (IBA1, green), lymphocytes (CD45, red), and nuclei (SYTO13, blue). **b** Volcano plot of significant abundantly expressed proteins detected in microglial nodules versus unaggregated microglia. **c** 20 × micropictograph confirming high expression of CD8 in CD45+ cells near microglial nodules. **d-g** Relative cell type marker expression **d** T-cell subtype marker expression **e** macrophage subtype marker expression **f** cell activation markers **g** in CD45+ ROIs for each patient
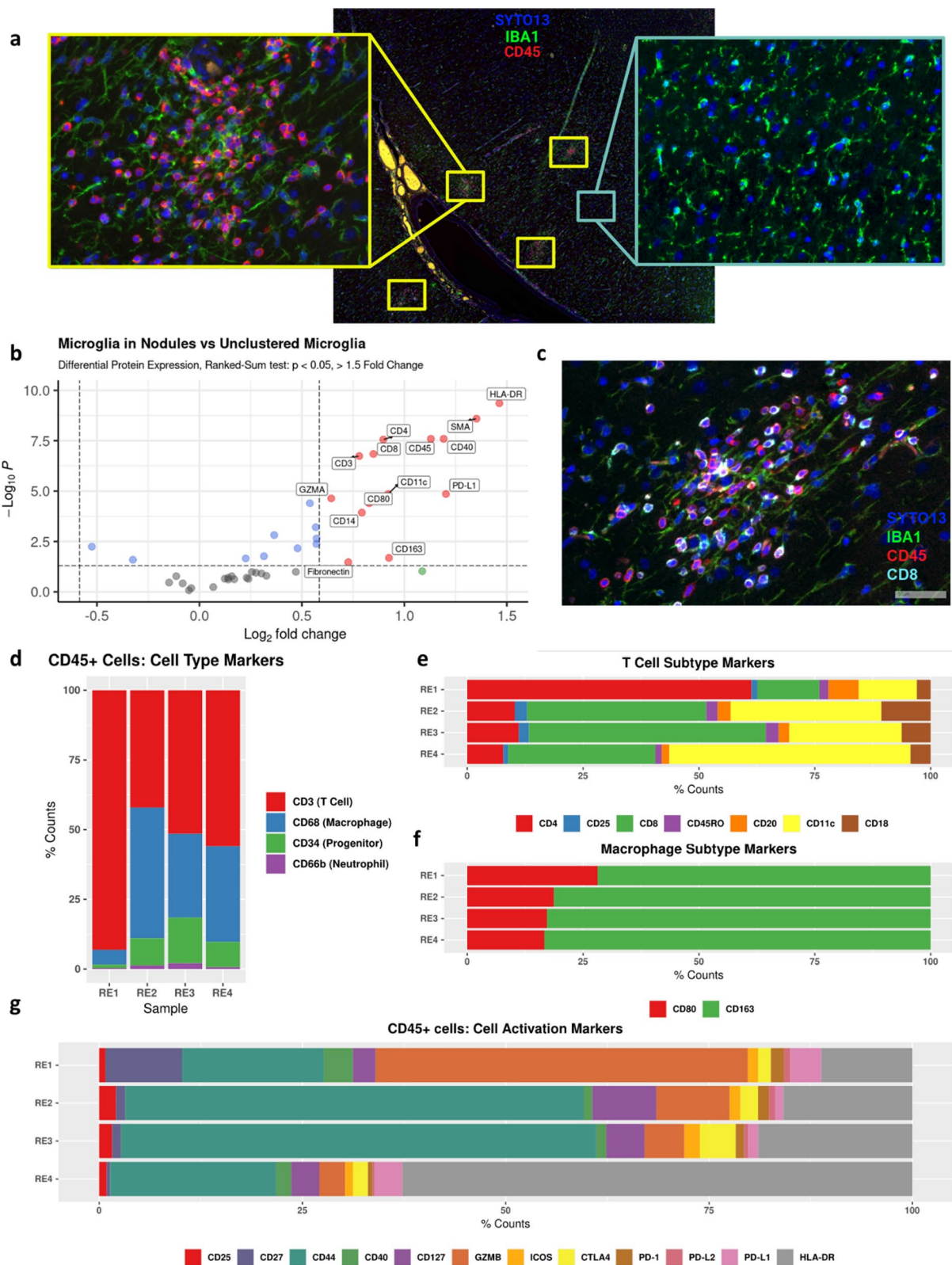
Fig. 4 (See legend on previous page.)

Fig. 4b-c). However, when analyzing expression of genes that regulate immune function or inflammation, particularly those highlighted in Fig. 3b, many are more abundantly expressed in RE microglia than in FCD or CTRL populations. Furthermore, our proteomic data demonstrate that the spatial organization of these microglial subpopulations is altered in the context of RE.

GO annotation enrichment analysis of microglia cluster DE genes revealed additional regulated biological processes beyond inflammation. Microglia in cluster 2 overexpress genes that regulate macrophage-derived foam cell differentiation, indicating that the microglia contain cellular debris, presumably from neurodegeneration. Although foamy microglia are common in multiple sclerosis (MS), another neurological disease due to immune-mediated pathogenesis [21, 68], these cells have not been analyzed in the context of RE. These cells could provide crucial spatiotemporal information about the neurodegenerative microenvironment of RE.

Other microglial subpopulations have similarities to microglial phenotypes studied in Alzheimer Disease (AD). Cluster 5 has abundantly high expression of FTL and FTH1, genes that encode for ferritin subunits. A similar iron-loading microglial phenotype, described by Kenkhuis et al., has been found in AD patients with high *β*-amyloid, high tau pathologies [27]. Two different clusters, 7 and 10, abundantly expressed genes such as *GRID2,* related to microglia-neuron crosstalk and the organization of synapse and postsynaptic organization. It is well documented that a major role of microglia is to regulate synaptic development and pruning, and dysregulation of these processes leads to inflammatory and epileptogenic disorders [4, 5]. Gerrits et al. described a similar microglial phenotype in the context of AD, particularly in tissue with tau pathology. These *GRID2*+ microglia were also enriched for gene ontology annotations related to neurotrophic functions like synapse organization and axonogenesis [19]. Understanding the role of these phenotypically related microglia across neurodegenerative diseases could offer insight into how microglia respond to neuroinflammatory pathologies. Microglia from cluster 7 and 10 also express genes that regulate *NMDA* receptor activity and are responsible for microglial process extension toward neurons during seizure, induced by increased global glutamate levels [16]. Additionally, these microglia abundantly express genes that regulate glutamate receptor signaling pathways and glutamatergic synaptic transmission. Several studies have shown that irregular glutamate levels and aberrant glutamatergic signaling lead to inflammation and epilepsy [8, 14]. Analysis of these microglia could offer insight into the transcriptomic landscape of epileptogenic microglia not just for RE, but for other disorders.

Pseudotime trajectory analysis of snRNA-Seq data suggests that while some microglial subpopulations have unique paths of differentiation from a homeostatic state, others may be temporally related along one or more differentiation trajectories. All trajectories from homeostasis to activated microglia, except one, travel through a common microglial population, cluster 0. All the microglia in cluster 0 have early to mid pseudotime scores and cluster 0 has no differentially high expression of genes. This suggests that the microglia in this cluster represent an initial differentiation state in which expression of homeostatic markers drops but inflammatory markers are not yet defined. In contrast, there are trajectories through multiple populations of inflammatory microglia, suggesting a temporal relationship mediated by cell signaling. A trajectory through clusters 3,2,1 emphasizes the role of both *NFKB1*, *CXCL10* and *WARS* as initiators of proinflammatory signaling, and their potential to affect function of nearby microglia [13, 32, 38]. Spatial autocorrelation in Monocle3 revealed PDEGs that had appreciable overlap with DEGs generated in Seurat. Interestingly, of the PDEGs with a top 20 Moran's I scores (Additional file 7: Fig. 7), five were DEGs highlighted in Fig. 3b as markers of immune regulation and inflammation. This correlation reinforces that in RE-affected microglia, the dominant drivers of microglial activation and deviation from homeostasis are modulators of immune response and inflammation. The top five PDEGs have differentially high expression in both clusters 8 and 10, however the expression occurs at different pseudotimes and the clusters are along different trajectories, indicating that functionally similar populations of microglia may have different activating drivers. Understanding the mechanisms of activation for disease-specific microglia across pseudotime trajectories can lead to novel targets for immune checkpoint therapeutics for neuroinflammatory disease.

While snRNA-seq provides transcriptome-wide data at single-cell resolution, it lacks spatial context and only infers in vivo protein abundance. Having high-plex, spatially-resolved proteomic data allowed us to further elaborate on the immunohistological data of Troscher et al. in two ways. First, we analyzed the differentially expressed proteins (DEPs) in microglial nodules. Second, we quantified the immune proteins of infiltrating CD45+ lymphocytes at microglial nodule locations. Microglial nodules consisted exclusively of IBA1+ cells with an activated, ameboid phenotype. Non-clustered microglia regions were selected to maximize homeostatic, ramified phenotypes. Not surprisingly, differential protein expression analysis revealed that HLA-DR, a classic marker of immune activation [56, 64], was expressed nearly threefold higher in clustered microglia versus

non-clustered. Other proinflammatory markers were also highly expressed in the nodules. CD40 is a microglial TNF receptor that is important in T-cell activation, stimulated by IFN-γ through the TNFα pathway, and has been implicated in other autoimmune disorders [12, 39]. Furthermore, when CD40 is bound to T-cell ligand CD40L, it promotes an increase in expression of CD80, another proinflammatory costimulatory molecule [65]. Alternatively, we see high relative expression of CD163 and MRC1, anti-inflammatory markers. Other DEPs have a more elusive role in the immune microenvironment of the nodules. PD-L1+ microglia have been shown to, in most cases, correlate with inhibition of CD8+ T-cells and reduce inflammation, although the mechanism of protection remains unclear [35]. Similarly, CD11c+ microglia have protective and regenerative effects in neuroinflammatory conditions [9]. CD14 has been shown to be an essential regulator of TLR4-mediated damage and disease response of microglia [24]. Our proteomic analysis provides spatial context for the dynamic mix of inflammatory signaling introduced by our single-nucleus transcriptomic analysis. Mapping the expression of genes that encode for nodule-enriched DEPs onto the microglia tSNE projection reveals that microglia in cluster 3 are most likely to be from a microglial nodule. This logically correlates with neuroinflammatory function of microglial nodules. Not only does cluster 3 have differentially high expression of *NFKB1*, *CXCL10, LIMK2* and *WARS*, all contributors to pro-inflammatory signaling [3, 13, 32, 38], but also the highest enrichment of GO annotations for positive regulation of immune response and cytokine, including type I interferon, production.

Immune targets for proteomic analysis of invading CD45+ lymphocytes were split into two groups, those that traditionally designate immune cell types and subtypes (Fig. 4d–f) and those that designate immune activation state (Fig. 4g). Although T-cell markers dominate the signal for CD45+ invading immune cells, there is evidence that invading monocyte-derived macrophages are present near the microglial nodules (Fig. 4d, f). Using the relative abundances of T-cell subtype and activation markers allows us to determine shifts in T-cell populations across samples. In RE4, based on CD3-CD8-CD4-CD11c expression, some of the lymphocytes are effector T-cells also known as cytotoxic T-cells (CTLs) [31] and others are likely a subset of regulatory T-cells (Tregs) shown to suppress CD4+ T-cells [49, 63]. RE2 and RE3 have similar protein expression profiles to RE4, however the lower CD11c expression and higher CD44 and suggest that the CTL:Treg ratio of present lymphocytes is higher [47]. In RE1 however, we observed much lower CD8 and CD44 expression, suggesting a lack of CTLs. Instead, we observed expanded expression of CD3, CD4

and GZMB. CD4+ GZMB+ T-cells have been shown to be a hallmark of several systemic autoimmune diseases and are associated with inflammation and tissue damage [45]. In addition to their helper and cytotoxic functions, these CD4+ T-cells are hypothesized to promote CD8+ T-cell effector processes via secreted cytokines [1]. Our analysis highlights the heterogeneity of patient immune response to RE and could help explain why immunotherapy has been largely ineffective in controlling RE progression [58].

Conclusions

These findings highlight the important role of microglia in the pathogenesis of Rasmussen encephalitis and confirm the significance of microglial nodules in promoting cytotoxic T-cell activity. Our work further underscores the advantages of technology, leveraging single-cell and spatial resolution for cell-type and location specific contributions to RE pathology. By performing multiomic analysis of disease affected microglia, we gain a deeper understanding of aberrant intra- and inter-cellular signaling leading to the progression of inflammation and neurotoxicity of RE. Our work ultimately demonstrates new and powerful methodologies that may guide future research toward elucidating the origin of RE pathogenesis and effective therapeutic intervention.

Abbreviations

RE: Rasmussen encephalitis; AD: Alzheimer disease; MS: Multiple sclerosis; snRNA-Seq: Single nucleus RNA sequencing; FCD: Focal cortical dysplasia; CTRL: Unaffected autopsy control; CTDS: Cell type diversity statistic; DEG: Differentially expressed gene; DEP: Differentially expressed protein; PDEG: Pseudotime differentially expressed gene; FFPE: Formalin -fixed, paraffin embedded; PBS: Phosphate buffered saline; FACS: Fluorescence-activated cell sorting; PCA: Principal component analysis; tSNE: T-distributed stochastic neighbor embedding; UMAP: Uniform manifold approximation and projection; MAST: Model-based analysis of single-cell transcriptomics; GO: Gene ontology; KEGG: Kyoto Encyclopedia of genes and genomes; FDR: False discovery rate; ROI: Region of interest.

Supplementary Information

Additional file 1. QC and cell typing for snRNA-seq data. **a**, **b** tSNE plots showing raw RNA and UMI counts per nucleus. **c**, **d** tSNE plots showing SCT-normalized RNA and UMI counts per nucleus. **e** tSNE plot showing mitochondrial transcript expression as a percent of total expression per nucleus. **f** Heatmap showing expression of common marker genes for annotated cell type. **g**, **h** Stacked bar graphs showing relative cell type per disease condition (**g**) and sample (**h**).

Additional file 2. Overlap of DEGs in RE relative to FCD and CTRL. a,b Venn diagrams showing the number of overlapping genes expressed differentially high (**a**) and differentially low (**b**) in RE vs CTRL and FCD. **c** Four-way plot showing FCD expression relative to RE vs CTRL expression relative to RE for each gene.

Additional file 3. Microglial markers and DEGs in microglial Louvain clusters. **a** tSNE plot of microglia showing all eleven Louvain clusters. **b** Violin

plots of top five most abundant differentially expressed genes in each microglial cluster, if applicable. **c** Violin plots illustrating the per-cluster expression of microglia-specific and homeostatic microglial markers.

Additional file 4. Sample and disease condition contribution to microglial clusters. **a** Side-by-side tSNE plot of microglia with accompanying stacked bar graph showing the percent of cells in cluster by sample. **b** tSNE plot of microglia in which each cell is colored by disease condition. **c** Stacked bar graph showing the percent of cells in disease condition by microglial cluster. **d** Box plot showing the distribution of cell type diversity statistics in each disease condition.

Additional file 5. Immune modulation and inflammation marker expression differs by disease condition. Ridge plots showing the expression of immune and inflammation markers highlighted in Figure 3, separated by disease condition with accompanying tSNE of microglia for reference.

Additional file 6. Pseudotime trajectory analysis. **a** UMAP plot of microglia showing all eleven Louvain clusters. **b** UMAP density plot showing the density of TMEM119 expression. Red star indicates root node for cell ordering. **c** UMAP plot showing pseudotime trajectories, where cells are colored by pseudotime score. Red star indicates root node for cell ordering. **d** Ridge plot displaying the pseudotime score of cells in each microglia cluster.

Additional file 7. Top PDEGs highlight diversity of pseudotime trajectories. Scatter plots of cells showing expression of top 20 PDEGs (by Moran's I score) vs pseudotime where cells are colored by microglial cluster. Red stars indicate gene is also an immune or inflammatory marker highlighted in Figure 3b.

Additional file 8. Nanostring GeoMx workflow and ROI segmenting. **a** Schematic detailing the workflow of the GeoMx digital spatial profiler platform. **b** 20x micropictographs displaying single channel CD45 and IBA1 images, the combined image, and how a typical ROI containing a microglial nodule was segmented by intensity thresholding.

Additional file 9. IBA1+ ROI segment protein expression. Heatmap showing protein expression of 42 protein targets in each IBA1+ ROI segment for each sample.

Additional file 10. CD45+ ROI segment protein expression. Heatmap showing protein expression of 42 protein targets in each CD45+ ROI segment for each sample.

Additional file 11. DEP gene expression in microglia snRNA-Seq. **a** Volcano plot of significant abundantly expressed proteins detected in microglial nodules versus unaggregated microglia. Red shape and labels highlight DEPs selected for single-nucleus microglia analysis. **b** tSNE density plots displaying gene expression density in microglia of markers selected in **a**. **c** tSNE density plot showing the expression density in microglia where all selected markers are expressed.

Additional file 12: Table S1. Differentially Expressed Genes in Microglia, RE vs CTRL.

Additional file 13: Table S2. Differentially Expressed Genes in Microglia, RE vs FCD.

Additional file 14: Table S3. Top Highly Differentially Expressed Genes in Microglia Subpopulations.

Additional file15: Table S4. Top 100 Differentially Expressed Genes Across Pseudotime Trajectories.

Author contributions
APO, JL, JAP, and DCK provided clinical data and patient samples. CRP and DRB performed pathological analysis of patient samples. JJW, TAB and KEM conceptualized research goals and methodology. WNS and JBN investigated frozen samples and generated single-nuclei transcriptomic data. JW and SS investigated FFPE samples and generated spatial proteomic data. JW and TAB performed formal analysis on transcriptomic and proteomic data, including data visualization. RKW and ERM provided equipment and resources. JW, TAB and KEM contributed to writing the manuscript. All authors read and approved the final manuscript.

Availability of data and materials
The datasets generated from this study are available from the corresponding author upon reasonable request.

Declarations

Ethics approval and consent to participate
Written informed consent for RE1, RE2, RE3, FCD1, and FCD2 was obtained in this study under a research protocol approved by the Institutional Review Board at Nationwide Children's Hospital (IRB18-00786). RE4, CTRL1, and CTRL2 tissues were obtained from external biobanks with proper documented consent.

Consent for publication
Not Applicable.

Competing interests
The authors declare no competing interests.

Author details
[1]The Steve and Cindy Rasmussen Institute for Genomic Medicine, Abigail Wexner Research Institute at Nationwide Children's Hospital, Research Building 3, 575 Children's Crossroad, Columbus, OH 43215, USA. [2]Department of Neurosurgery, Nationwide Children's Hospital, Columbus, OH, USA. [3]Department of Neurosurgery, The Ohio State University College of Medicine, Columbus, OH, USA. [4]Department of Pathology, The Ohio State University College of Medicine, Columbus, OH, USA. [5]Department of Pathology and Laboratory Medicine, Nationwide Children's Hospital, Columbus, OH, USA. [6]Department of Biomedical Education and Anatomy, Division of Anatomy, The Ohio State University College of Medicine, Columbus, OH, USA. [7]Department of Pediatrics, The Ohio State University College of Medicine, 700 Children's Dr., Columbus, Oh 43205, USA. [8]Division of Child Neurology, Nationwide Children's Hospital, Columbus, OH, USA.

References
1. Al Nimer F, Jelcic I, Kempf C, Pieper T, Budka H, Sospedra M, Martin R (2018) Phenotypic and functional complexity of brain-infiltrating T cells in Rasmussen encephalitis. Neurol Neuroimmunol Neuroinflamm 5:e419. https://doi.org/10.1212/NXI.0000000000000419
2. Alquicira-Hernandez J, Powell JE (2021) Nebulosa recovers single-cell gene expression signals by kernel density estimation. Bioinformatics 37:2485–2487. https://doi.org/10.1093/bioinformatics/btab003
3. Alsegiani AS, Shah ZA (2020) The role of cofilin in age-related neuroinflammation. Neural Regen Res 15:1451–1459. https://doi.org/10.4103/1673-5374.274330
4. Andoh M, Ikegaya Y, Koyama R (2019) Synaptic pruning by microglia in epilepsy. J Clin Med 8:2170. https://doi.org/10.3390/jcm8122170
5. Andoh M, Koyama R (2021) Microglia regulate synaptic development and plasticity. Dev Neurobiol 81:568–590. https://doi.org/10.1002/dneu.22814
6. Audrito V, Messana VG, Deaglio S (2020) NAMPT and NAPRT: two metabolic enzymes with key roles in inflammation. Front Oncol 10:358. https://doi.org/10.3389/fonc.2020.00358

7. Bakken TE, Jorstad NL, Hu Q, Lake BB, Tian W, Kalmbach BE, Crow M, Hodge RD, Krienen FM, Sorensen SA et al (2021) Comparative cellular analysis of motor cortex in human, marmoset and mouse. Nature 598:111–119. https://doi.org/10.1038/s41586-021-03465-8

8. Barker-Haliski M, White HS (2015) Glutamatergic mechanisms associated with seizures and epilepsy. Cold Spring Harb Perspect Med 5:a022863. https://doi.org/10.1101/cshperspect.a022863

9. Benmamar-Badel A, Owens T, Wlodarczyk A (2020) Protective microglial subset in development, aging, and disease: lessons from transcriptomic studies. Front Immunol 11:430. https://doi.org/10.3389/fimmu.2020.00430

10. Bien CG, Tiemeier H, Sassen R, Kuczaty S, Urbach H, von Lehe M, Becker AJ, Bast T, Herkenrath P, Karenfort M et al (2013) Rasmussen encephalitis: incidence and course under randomized therapy with tacrolimus or intravenous immunoglobulins. Epilepsia 54:543–550. https://doi.org/10.1111/epi.12042

11. Cepeda C, Chang JW, Owens GC, Huynh MN, Chen JY, Tran C, Vinters HV, Levine MS, Mathern GW (2015) In Rasmussen encephalitis, hemichannels associated with microglial activation are linked to cortical pyramidal neuron coupling: a possible mechanism for cellular hyperexcitability. CNS Neurosci Ther 21:152–163. https://doi.org/10.1111/cns.12352

12. Chitnis T, Khoury SJ (2003) Role of costimulatory pathways in the pathogenesis of multiple sclerosis and experimental autoimmune encephalomyelitis. J Allergy Clin Immunol 112(837–849):850. https://doi.org/10.1016/j.jaci.2003.08.025

13. Clarner T, Janssen K, Nellessen L, Stangel M, Skripuletz T, Krauspe B, Hess F-M, Denecke B, Beutner C, Linnartz-Gerlach B et al (2015) CXCL10 triggers early microglial activation in the cuprizone model. J Immunol 194:3400–3413. https://doi.org/10.4049/jimmunol.1401459

14. Czapski GA, Strosznajder JB (2021) Glutamate and GABA in microglia-neuron cross-talk in Alzheimer's disease. Int J Mol Sci 22:11677. https://doi.org/10.3390/ijms222111677

15. Eden E, Navon R, Steinfeld I, Lipson D, Yakhini Z (2009) GOrilla: a tool for discovery and visualization of enriched GO terms in ranked gene lists. BMC Bioinformatics 10:48. https://doi.org/10.1186/1471-2105-10-48

16. Eyo UB, Peng J, Swiatkowski P, Mukherjee A, Bispo A, Wu LJ (2014) Neuronal hyperactivity recruits microglial processes via neuronal NMDA receptors and microglial P2Y12 receptors after status epilepticus. J Neurosci 34:10528–10540. https://doi.org/10.1523/JNEUROSCI.0416-14.2014

17. Fauser S, Elger CE, Woermann F, Bien CG (2022) Rasmussen encephalitis: Predisposing factors and their potential role in unilaterality. Epilepsia 63:108–119. https://doi.org/10.1111/epi.17131

18. Finak G, McDavid A, Yajima M, Deng J, Gersuk V, Shalek AK, Slichter CK, Miller HW, McElrath MJ, Prlic M et al (2015) MAST: a flexible statistical framework for assessing transcriptional changes and characterizing heterogeneity in single-cell RNA sequencing data. Genome Biol 16:278. https://doi.org/10.1186/s13059-015-0844-5

19. Gerrits E, Brouwer N, Kooistra SM, Woodbury ME, Vermeiren Y, Lambourne M, Mulder J, Kummer M, Moller T, Biber K et al (2021) Distinct amyloid-beta and tau-associated microglia profiles in Alzheimer's disease. Acta Neuropathol 141:681–696. https://doi.org/10.1007/s00401-021-02263-w

20. Ghaleb AM, Bialkowska AB, Snider AJ, Gnatenko DV, Hannun YA, Yang VW, Schmidt VA (2015) IQ motif-containing GTPase-activating protein 2 (IQGAP2) Is a novel regulator of colonic inflammation in mice. PLoS ONE 10:e0129314. https://doi.org/10.1371/journal.pone.0129314

21. Grajchen E, Hendriks JJA, Bogie JFJ (2018) The physiology of foamy phagocytes in multiple sclerosis. Acta Neuropathol Commun 6:124. https://doi.org/10.1186/s40478-018-0628-8

22. Hafemeister C, Satija R (2019) Normalization and variance stabilization of single-cell RNA-seq data using regularized negative binomial regression. Genome Biol 20:296. https://doi.org/10.1186/s13059-019-1874-1

23. Hao Y, Hao S, Andersen-Nissen E, Mauck WM 3rd, Zheng S, Butler A, Lee MJ, Wilk AJ, Darby C, Zager M et al (2021) Integrated analysis of multimodal single-cell data. Cell 184(3573–3587):e3529. https://doi.org/10.1016/j.cell.2021.04.048

24. Janova H, Bottcher C, Holtman IR, Regen T, van Rossum D, Gotz A, Ernst AS, Fritsche C, Gertig U, Saiepour N et al (2016) CD14 is a key organizer of microglial responses to CNS infection and injury. Glia 64:635–649. https://doi.org/10.1002/glia.22955

25. Kanehisa M, Sato Y, Kawashima M (2022) KEGG mapping tools for uncovering hidden features in biological data. Protein Sci 31:47–53. https://doi.org/10.1002/pro.4172

26. Karagiannis TT, Monti S, Sebastiani P (2022) Cell type diversity statistic: an entropy-based metric to compare overall cell type composition across samples. Front Genet 13:855076. https://doi.org/10.3389/fgene.2022.855076

27. Kenkhuis B, Somarakis A, de Haan L, Dzyubachyk O, ME IJ, de Miranda N, Lelieveldt BPF, Dijkstra J, van Roon-Mom WMC, Hollt T, et al (2021) Iron loading is a prominent feature of activated microglia in Alzheimer's disease patients. Acta Neuropathol Commun 9:27. https://doi.org/10.1186/s40478-021-01126-5

28. Kim JE, Ryu HJ, Kim MJ, Kang TC (2014) LIM kinase-2 induces programmed necrotic neuronal death via dysfunction of DRP1-mediated mitochondrial fission. Cell Death Differ 21:1036–1049. https://doi.org/10.1038/cdd.2014.17

29. Koboldt DC, Miller KE, Miller AR, Bush JM, McGrath S, Leraas K, Crist E, Fair S, Schwind W, Wijeratne S et al (2021) PTEN somatic mutations contribute to spectrum of cerebral overgrowth. Brain 144:2971–2978. https://doi.org/10.1093/brain/awab173

30. Kowal K, Silver R, Slawinska E, Bielecki M, Chyczewski L, Kowal-Bielecka O (2011) CD163 and its role in inflammation. Folia Histochem Cytobiol 49:365–374. https://doi.org/10.5603/fhc.2011.0052

31. Lee-Sayer SSM, Maeshima N, Dougan MN, Dahiya A, Arif AA, Dosanjh M, Maxwell CA, Johnson P (2018) Hyaluronan-binding by CD44 reduces the memory potential of activated murine CD8 T cells. Eur J Immunol 48:803–814. https://doi.org/10.1002/eji.201747263

32. Liu T, Zhang L, Joo D, Sun SC (2017) NF-kappaB signaling in inflammation. Signal Transduct Target Ther 2:17023. https://doi.org/10.1038/sigtrans.2017.23

33. Love MI, Huber W, Anders S (2014) Moderated estimation of fold change and dispersion for RNA-seq data with DESeq2. Genome Biol 15:550. https://doi.org/10.1186/s13059-014-0550-8

34. Luan G, Gao Q, Zhai F, Chen Y, Li T (2016) Upregulation of HMGB1, toll-like receptor and RAGE in human Rasmussen's encephalitis. Epilepsy Res 123:36–49. https://doi.org/10.1016/j.eplepsyres.2016.03.005

35. Manenti S, Orrico M, Masciocchi S, Mandelli A, Finardi A, Furlan R (2022) PD-1/PD-L axis in neuroinflammation: new insights. Front Neurol 13:877936. https://doi.org/10.3389/fneur.2022.877936

36. McGinnis CS, Murrow LM, Gartner ZJ (2019) doubletfinder: doublet detection in single-cell RNA sequencing data using artificial nearest neighbors. Cell Syst 8(329–337):e324. https://doi.org/10.1016/j.cels.2019.03.003

37. Muzio L, Viotti A, Martino G (2021) Microglia in Neuroinflammation and neurodegeneration: from understanding to therapy frontiers in neuroscience. Frontiers Media SA, City.

38. Nguyen TTT, Yoon HK, Kim YT, Choi YH, Lee WK, Jin M (2020) Tryptophanyl-tRNA synthetase 1 signals activate TREM-1 via TLR2 and TLR4. Biomolecules 10:1283. https://doi.org/10.3390/biom10091283

39. Nguyen VT, Benveniste EN (2002) Critical role of tumor necrosis factor-alpha and NF-kappa B in interferon-gamma -induced CD40 expression in microglia/macrophages. J Biol Chem 277:13796–13803. https://doi.org/10.1074/jbc.M111906200

40. Oliveira-Nascimento L, Massari P, Wetzler LM (2012) The role of TLR2 in infection and immunity. Front Immunol 3:79. https://doi.org/10.3389/fimmu.2012.00079

41. Orsini A, Foiadelli T, Carli N, Costagliola G, Masini B, Bonuccelli A, Savasta S, Peroni D, Consolini R, Striano P (2020) Rasmussen's encephalitis: from immune pathogenesis towards targeted-therapy. Seizure 81:76–83. https://doi.org/10.1016/j.seizure.2020.07.023

42. Owens GC, Chang JW, Huynh MN, Chirwa T, Vinters HV, Mathern GW (2016) Evidence for resident memory T cells in Rasmussen encephalitis. Front Immunol 7:64. https://doi.org/10.3389/fimmu.2016.00064

43. Owens GC, Huynh MN, Chang JW, McArthur DL, Hickey MJ, Vinters HV, Mathern GW, Kruse CA (2013) Differential expression of interferon-gamma and chemokine genes distinguishes Rasmussen encephalitis from cortical dysplasia and provides evidence for an early Th1 immune response. J Neuroinflammation 10:56. https://doi.org/10.1186/1742-2094-10-56

44. Pardo CA, Vining EP, Guo L, Skolasky RL, Carson BS, Freeman JM (2004) The pathology of Rasmussen syndrome: stages of cortical involvement

and neuropathological studies in 45 hemispherectomies. Epilepsia 45:516–526. https://doi.org/10.1111/j.0013-9580.2004.33103.x

45. Park S, Anderson NL, Canaria DA, Olson MR (2021) Granzyme-producing CD4 T cells in cancer and autoimmune disease. Immunohorizons 5:909–917. https://doi.org/10.4049/immunohorizons.2100017

46. Qiu X, Mao Q, Tang Y, Wang L, Chawla R, Pliner HA, Trapnell C (2017) Reversed graph embedding resolves complex single-cell trajectories. Nat Methods 14:979–982. https://doi.org/10.1038/nmeth.4402

47. Rafi-Janajreh AQ, Nagarkatti PS, Nagarkatti M (1998) Role of CD44 in CTL and NK cell activity. Front Biosci 3:d665-671. https://doi.org/10.2741/a311

48. Rasmussen T, Olszewski J, Lloydsmith D (1958) Focal seizures due to chronic localized encephalitis. Neurology 8:435–445. https://doi.org/10.1212/wnl.8.6.435

49. Rostamzadeh D, Haghshenas MR, Daryanoosh F, Samadi M, Hosseini A, Ghaderi A, Mojtahedi Z, Babaloo Z (2019) Altered frequency of CD8(+) CD11c(+) T cells and expression of immunosuppressive molecules in lymphoid organs of mouse model of colorectal cancer. J Cell Physiol 234:11986–11998. https://doi.org/10.1002/jcp.27856

50. Roszer T (2015) Understanding the mysterious M2 macrophage through activation markers and effector mechanisms. Mediators Inflamm 2015:816460. https://doi.org/10.1155/2015/816460

51. Schirmer L, Velmeshev D, Holmqvist S, Kaufmann M, Werneburg S, Jung D, Vistnes S, Stockley JH, Young A, Steindel M et al (2019) Neuronal vulnerability and multilineage diversity in multiple sclerosis. Nature 573:75–82. https://doi.org/10.1038/s41586-019-1404-z

52. Schneider-Hohendorf T, Mohan H, Bien CG, Breuer J, Becker A, Gorlich D, Kuhlmann T, Widman G, Herich S, Elpers C et al (2016) CD8(+) T-cell pathogenicity in Rasmussen encephalitis elucidated by large-scale T-cell receptor sequencing. Nat Commun 7:11153. https://doi.org/10.1038/ncomms11153

53. Schwab N, Bien CG, Waschbisch A, Becker A, Vince GH, Dornmair K, Wiendl H (2009) CD8+ T-cell clones dominate brain infiltrates in Rasmussen encephalitis and persist in the periphery. Brain 132:1236–1246. https://doi.org/10.1093/brain/awp003

54. Schwabenland M, Bruck W, Priller J, Stadelmann C, Lassmann H, Prinz M (2021) Analyzing microglial phenotypes across neuropathologies: a practical guide. Acta Neuropathol 142:923–936. https://doi.org/10.1007/s00401-021-02370-8

55. Squair JW, Gautier M, Kathe C, Anderson MA, James ND, Hutson TH, Hudelle R, Qaiser T, Matson KJE, Barraud Q et al (2021) Confronting false discoveries in single-cell differential expression. Nat Commun 12:5692. https://doi.org/10.1038/s41467-021-25960-2

56. Swanson MEV, Murray HC, Ryan B, Faull RLM, Dragunow M, Curtis MA (2020) Quantitative immunohistochemical analysis of myeloid cell marker expression in human cortex captures microglia heterogeneity with anatomical context. Sci Rep 10:11693. https://doi.org/10.1038/s41598-020-68086-z

57. Syed MM, Phulwani NK, Kielian T (2007) Tumor necrosis factor-alpha (TNF-alpha) regulates Toll-like receptor 2 (TLR2) expression in microglia. J Neurochem 103:1461–1471. https://doi.org/10.1111/j.1471-4159.2007.04838.x

58. Tang C, Luan G, Li T (2020) Rasmussen's encephalitis: mechanisms update and potential therapy target. Ther Adv Chronic Dis 11:2040622320971413. https://doi.org/10.1177/2040622320971413

59. Traag VA, Waltman L, van Eck NJ (2019) From Louvain to Leiden: guaranteeing well-connected communities. Sci Rep 9:5233. https://doi.org/10.1038/s41598-019-41695-z

60. Troscher AR, Wimmer I, Quemada-Garrido L, Kock U, Gessl D, Verberk SGS, Martin B, Lassmann H, Bien CG, Bauer J (2019) Microglial nodules provide the environment for pathogenic T cells in human encephalitis. Acta Neuropathol 137:619–635. https://doi.org/10.1007/s00401-019-01958-5

61. Van der Maaten L, Hinton G (2008) Visualizing data using t-SNE. J Mach Learn Res 9(11):2579–2605. http://jmlr.org/papers/v9/vandermaaten08a.html

62. Varadkar S, Bien CG, Kruse CA, Jensen FE, Bauer J, Pardo CA, Vincent A, Mathern GW, Cross JH (2014) Rasmussen's encephalitis: clinical features, pathobiology, and treatment advances. Lancet Neurol 13:195–205. https://doi.org/10.1016/S1474-4422(13)70260-6

63. Vinay DS, Kwon BS (2010) CD11c+CD8+ T cells: two-faced adaptive immune regulators. Cell Immunol 264:18–22. https://doi.org/10.1016/j.cellimm.2010.05.010

64. Walker DG, Lue LF (2015) Immune phenotypes of microglia in human neurodegenerative disease: challenges to detecting microglial polarization in human brains. Alzheimers Res Ther 7:56. https://doi.org/10.1186/s13195-015-0139-9

65. Yang I, Han SJ, Kaur G, Crane C, Parsa AT (2010) The role of microglia in central nervous system immunity and glioma immunology. J Clin Neurosci 17:6–10. https://doi.org/10.1016/j.jocn.2009.05.006

66. Yang S, Wang J, Brand DD, Zheng SG (2018) Role of TNF-TNF receptor 2 signal in regulatory T cells and its therapeutic implications. Front Immunol 9:784. https://doi.org/10.3389/fimmu.2018.00784

67. Zhou Y, Cui C, Ma X, Luo W, Zheng SG, Qiu W (2020) Nuclear factor kappaB (NF-kappaB)-mediated inflammation in multiple sclerosis. Front Immunol 11:391. https://doi.org/10.3389/fimmu.2020.00391

68. Zierfuss B, Weinhofer I, Buda A, Popitsch N, Hess L, Moos V, Hametner S, Kemp S, Kohler W, Forss-Petter S et al (2020) Targeting foam cell formation in inflammatory brain diseases by the histone modifier MS-275. Ann Clin Transl Neurol 7:2161–2177. https://doi.org/10.1002/acn3.51200

Publisher's Note